

Local Energy Gap in Deformed Carbon Nanotubes

K. Sasaki and Y. Kawazoe

Institute for Materials Research, Tohoku University, Sendai 980-8577, Japan

R. Saito

Department of Physics, Tohoku University and CREST, JST, Sendai 980-8578, Japan

(Dated: May 22, 2019)

Effects of geometrical deformation of the graphite surface on the dynamics of the conducting electrons are investigated theoretically within the framework of a deformation-induced gauge field and corresponding deformation-induced magnetic field, which gives a local energy gap along the axis of the deformed nanotube. We compare our results of the energy gap with some experimental data of energy gap in nanotubes and pea-pod. We also discuss a mixing of two Fermi points and construct a general model of low energy dynamics including a short-range deformation of the graphite sheet. The derived model is equivalent to the Weyl equation in the U(1) and SU(2) non-Abelian deformation-induced gauge fields.

I. INTRODUCTION

Geometrical structure of materials and their electronic or magnetic properties are closely related to each other, and it is widely recognized that carbon nanotubes [1] provide us with a great opportunity to study such a relationship. For instance, a single wall carbon nanotube (SWNT) exhibits metallic or semiconducting behavior depending on the lattice structure around the tube axis [2, 3]. Carbon nanotube is a graphene sheet folded up into a cylinder and deformation of the graphite surface changes the dynamics of the conducting electrons through the modification of the overlap integral of nearest-neighbor orbitals. The energy dispersion relation of the graphite surface is unique because of the linear dispersion relation at the two distinct Fermi points (K and K' point). The linear energy dispersion relation with the honeycomb lattice structure leads to the Weyl equation [4]. In this case, the perturbation due to the atomic deformation appears in the dynamics through the gauge coupling [5]. A conducting electron moves on the deformed graphene sheet in which the deformation can be expressed by deformation-induced gauge field. The effect of finite curvature on the low energy dynamics was clarified by Kane and Mele [5]. They showed that the curvature effect can be included as an effective gauge field which gives a shift of the Fermi point in the Brillouin zone through the Aharonov-Bohm effect. Their theoretical result of the energy gap induced by the curvature effect was proved by a scanning tunneling spectroscopy (STS) experiment of Ouyang et al. [6] and was applied to different chiral structures by several authors [7]. In the present paper, we generalize the idea of the effective gauge field to a local deformation of the graphene surface.

In this paper, we clarify how the dynamics of the electron depends on the geometry of a deformed surface in sections II and III. Especially, we consider how local deformation affects the local electric properties of the conducting electrons of SWNTs in terms of the deformation-induced gauge field. It should be mentioned here that the

deformation-induced gauge field and the usual electromagnetic gauge field are different from each other, though we can use analogy in many cases. Furthermore the deformation-induced magnetic field does not concern the spin of an electron but pseudo-spin [8] defined by the two sublattices of graphite and SWNTs. In section IV, the relationship of the atomic deformation with a local energy gap structure is clarified. We compare our theoretical result with the local energy gap observed by STS in nanotubes [6] and pea-pod [9]. In section V, we will consider a short range deformation that results in a mixing of the wave functions at two Fermi points and construct an effective model for the low energy dynamics.

II. DEFINITION OF GAUGE FIELD FOR DEFORMATION

Quantum behavior of the conducting electrons on a graphene surface is described by the following nearest-neighbor tight-binding Hamiltonian:

$$H_{\text{near}} = \sum_{\substack{\mathbf{X} \\ \mathbf{X}}} V_a(\mathbf{r}_i) a_{i+a}^{\dagger} a_i + h.c.; \quad (1)$$

where A in the summation index denotes A-sublattice, a_i and a_i^{\dagger} are canonical annihilation-creation operators of the electron at the site i that satisfy the anti-commutation relation: $[a_i, a_j^{\dagger}] = \delta_{ij}$, and the site $i+a$ indicates the nearest-neighbor sites ($a \in \{1, 2, 3\}\mathbf{g}$). We have included deformation on the graphene surface as the position-dependent hopping integral $V_a(\mathbf{r}_i)$ in the Hamiltonian. We decompose the hopping integral into two components: $V_a(\mathbf{r}_i) = V + V_a(\mathbf{r}_i)$, and define $H_{\text{near}} = H_0 + H_{\text{deform}}$ where

$$H_0 = \sum_{\substack{\mathbf{X} \\ \mathbf{X}}} V a_{i+a}^{\dagger} a_i + h.c.; \quad (2)$$

$$H_{\text{deform}} = \sum_{\substack{\mathbf{X} \\ \mathbf{X}}} V_a(\mathbf{r}_i) a_{i+a}^{\dagger} a_i + h.c.; \quad (3)$$

Hereafter we call H_{deform} the deformed Hamitonian. The total Hamitonian adopted in this paper is $H_{\text{near}} = H_0 + H_{\text{deform}}$, which is not easy to solve for general $V_a(r_i)$. However, as far as we consider the physics near the Fermi level, one can obtain several important physical consequences. For example, the model Hamitonian can exhibit a local energy gap [9] for a specific deformation $V_a(r_i)$.

We follow the effective-mass description [10] of the low energy conducting electrons around the Fermi level. Here we first consider the case that the deformation is sufficiently delocalized compared with the diameter of a SWNT so that there is no interaction between two Fermi points. In this case we have doubly degenerate electronic states near K and K' points. The effective Hamitonian at K -point H_K is given by

$$H_K = v_F (\mathbf{p} \cdot \mathbf{A}); \quad (4)$$

where we have denoted $\mathbf{p} = p_1 \hat{\mathbf{p}}_1 + p_2 \hat{\mathbf{p}}_2$ and $\mathbf{A} = A_1 \hat{\mathbf{A}}_1 + A_2 \hat{\mathbf{A}}_2$, where \mathbf{A} is a vector field defined on the surface, v_F is the Fermi velocity, and $\hat{\mathbf{p}}_i$ ($i = 1, 2, 3$) are the Pauli matrices:

$$\hat{\mathbf{p}}_1 = \begin{pmatrix} 0 & 1 \\ 1 & 0 \end{pmatrix}; \quad \hat{\mathbf{p}}_2 = \begin{pmatrix} 0 & i \\ i & 0 \end{pmatrix}; \quad \hat{\mathbf{p}}_3 = \begin{pmatrix} 1 & 0 \\ 0 & 1 \end{pmatrix}; \quad (5)$$

Notice that we denote the coordinate around (along) the axis $x_1(x_2)$. The first term $v_F \mathbf{p}$ describes the dispersion of H_0 [4], and the second term $v_F \mathbf{A}$ denotes that of the deformed Hamitonian and the field $v_F \mathbf{A}(\mathbf{r})$ is given by a linear function of $V_a(\mathbf{r})$. We will show an explicit form for $\mathbf{A}(\mathbf{r})$ in the next section but here we note the following points: (1) The deformation can be included as a gauge field because of the gauge coupling: $\mathbf{p} \cdot \mathbf{A}$. We call \mathbf{A} the deformation-induced gauge field and distinguish it from the electromagnetic gauge field \mathbf{A}^{em} . Note that \mathbf{A} does not break time-reversal ($T \rightarrow T$) symmetry because the sign in front of \mathbf{A} has a different sign at K and K' points, which is contrasted with the T -violating nature of \mathbf{A}^{em} (see Eq. 22). (2) It is possible to decompose any gauge field into the sum of a constant, rotation-less, and divergence-less component as

$$\mathbf{A}_i = \mathbf{A}_i^0 + \theta_i \mathbf{a} + \epsilon_{ij} \theta_j \mathbf{b}; \quad i, j = 1, 2; \quad (6)$$

where ϵ_{ij} is the antisymmetric tensor ($\epsilon_{12} = \epsilon_{21} = 1$), and \mathbf{a} and \mathbf{b} are regular scalar functions defined on the tube surface.

Several important physical informations can be derived from H_K through the dimensional reduction: we integrate H_K over the circumference coordinate (x_1) to obtain a one-dimensional theory:

$$I \frac{dx_1}{C_h} H_K = v_F (\mathbf{p}_1^0 \cdot \mathbf{A}_1^0 - m(x_2))_1 + v_F (\mathbf{p}_2 \cdot \mathbf{A}_2^0)_2; \quad (7)$$

where C_h is the circumference length, \mathbf{p}_1^0 is determined by the chiral index, and

$$I m(x_2) = \frac{dx_1}{C_h} \theta_2 \mathbf{a}(x_1; x_2); \quad (8)$$

Note that the function \mathbf{a} for A_1 disappears by the integration over x_1 -coordinate. We have neglected the \mathbf{a} part for A_2 because it can be absorbed by a phase of the wave function. We identify the A_1 term with the mass of a particle propagating along the axis direction (x_2). This is because (1) the energy spectrum at position x_2 is bounded by the square root of the sum of square of each coefficient of the Pauli matrices in Eq.(7):

$$\frac{q}{\sqrt{(\mathbf{p}_1^0 \cdot \mathbf{A}_1^0 - m(x_2))^2 + (\mathbf{p}_2 \cdot \mathbf{A}_2^0)^2}}; \quad (9)$$

and (2) p_2 scales as inverse of the system length ($l = \frac{C_h}{2\pi}$) and hence $p_2 \cdot A_2^0$ can be neglected as compared with the $\mathbf{p}_1^0 \cdot \mathbf{A}_1^0 - m(x_2)$ for a long system ($C_h \gg l$). We define a local energy gap as the minimum energy gap for long tubes:

$$\begin{aligned} E_{\text{gap}}(x_2) &= 2v_F \frac{\mathbf{p}_1^0 \cdot \mathbf{A}_1^0 - m(x_2)}{l} \\ &= 2v_F \frac{\mathbf{p}_1^0}{C_h} \frac{dx_1}{l} A_1(x_1; x_2); \end{aligned} \quad (10)$$

Since the circumferential component (A_1) of the deformation-induced gauge field is determined by the modulation part of the hopping integral, by knowing $V_a(\mathbf{r})$ one can calculate the local energy gap using the above formula. The modulation part of the hopping integral can be calculated by choosing a specific scheme. We will adopt the Slater-Koster scheme and apply the formula to several deformed nanotubes. In the next section, we shall give a detailed derivation and present a general formula which is applicable to an arbitrary chiral index.

III. DERIVATION OF THE LOCAL ENERGY GAP

Here we show an explicit form of \mathbf{A} by $V_a(r_i)$. First, we rewrite Eq.(2) using the Bloch basis vector as

$$H_0 = V \sum_k f(k) j_A^k i h_B^k j + h.c.; \quad (11)$$

where we have defined $f(k) = \sum_a f_a(k)$ and $f_a(k) = e^{ik \cdot R_a}$, and R_a ($a = 1, 2, 3$) are vectors pointing to the nearest neighbor sites of an A-site (Fig. 1). We have defined the Bloch basis vectors with wave vector k as

$$j^k_i = \frac{1}{N} \sum_{i2}^X e^{ik \cdot r_{i2}} a_{i2}^k j_i; \quad (12)$$

where $i = A, B$ indices denote two sublattices which are illustrated in Fig. 1, and N_A ($= N_B$) denotes the number of black (white) sites in solid. Here r_i labels the vector pointing each site i . H_0 consists of only momentum preserving interactions ($k \rightarrow k$) because of the translational symmetries. However, H_{deform} contains momentum transferring term ($k \rightarrow k + \mathbf{q}$).

We expand Eq.(11) around the K -point k_F ,

$$H_0 = V \sum_a f_a(k_F) i(k - k_F) R j_A^k i h_B^k j + h.c.; \quad (13)$$

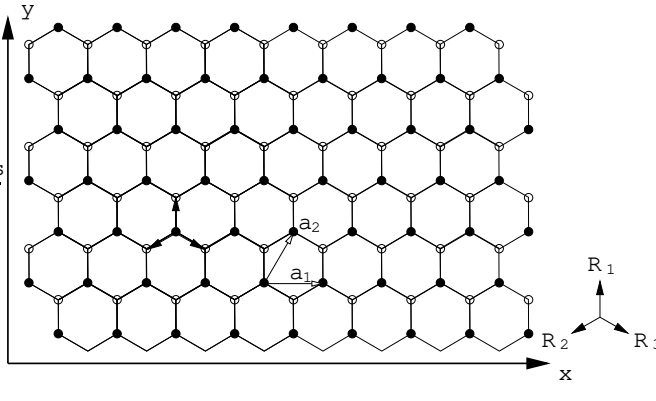


FIG. 1: Lattice structure of the honeycomb lattice, which possesses two symmetry translation vectors: $a_1 = \frac{3a_{cc}}{2}e_x + \frac{3a_{cc}}{2}e_y$ and $a_2 = (-\frac{3}{2})a_{cc}e_x + (\frac{3}{2})a_{cc}e_y$, where e_x and e_y are unit vectors, and a_{cc} is the nearest neighbor bond length. The black (white)-circle indicates A (B)-sublattice. The vectors R_a ($a = 2, 1, 2, 3$) are vectors pointing to the nearest neighbor sites of an A-site. They are given by $R_1 = a_{cc}e_y$; $R_2 = (-\frac{3}{2})a_{cc}e_x$; $R_3 = (\frac{3}{2})a_{cc}e_x$.

where we have used the following constraint: $\int_a f_a(k_F) = 0$ (one may set $f_1(k_F) = 1$; $f_2(k_F) = e^{i\frac{2\pi}{3}}$, and $f_3(k_F) = e^{+i\frac{2\pi}{3}}$). The lattice structure of SWNTs is specified by the chiral and translational vectors defined by $C_h = n a_1 + m a_2$ and $T = p a_1 + q a_2$, where a_1 and a_2 are symmetry translation vectors on the planar honeycomb lattice (Fig. 1). The corresponding wave vector k can be decomposed as $k = k_1 + k_2$, where k_1 and k_2 are integer coefficients of vectors k_1 and k_2 that satisfy $C_h \cdot k = 2$; $C_h \cdot k = 0$; $T \cdot k = 0$; $T \cdot k = 2$. With these definitions, the first term of the right hand side of Eq.(13) is given by

$$V e^{i w j_A^k i h_B^k j} \quad (14)$$

where $w = w_1 - iw_2$, and w_1 and w_2 are

$$w_1 = \frac{3a_{cc}}{2\mathcal{C}_h j} (2 - 1 - k_F - \zeta); \quad w_2 = \frac{3a_{cc}}{2\mathcal{C}_h j} (2 - 2 - k_F - T); \quad (15)$$

and the angle satisfies

$$n + \frac{m}{2} - \frac{p}{2} - \frac{q}{2} = \frac{\mathcal{C}_h j}{3a_{cc}} e^{i\pi} : \quad (16)$$

To obtain Eq.(14), it is useful to rewrite R_a in terms of the chiral and translational vectors:

$$\begin{aligned} R_1 &= \frac{2}{3N_c} h p + \frac{q}{2} C_h + n + \frac{m}{2} T; \\ R_2 &= \frac{2}{3N_c} h p - \frac{q}{2} C_h + \frac{n - m}{2} T; \\ R_3 &= \frac{2}{3N_c} h p + q C_h + \frac{n}{2} + m T; \end{aligned} \quad (17)$$

where we have introduced $N_c = m p - n q$ and used the following relationship: $(3 - 3 - 2)a_{cc}^2 N_c = \mathcal{C}_h j T$. Finally,

the Hamiltonian matrix for H_0 can be expressed at the K-point in the basis of two sublattices $(A; B)^t$ by

$$H_0 = V \begin{pmatrix} 0 & e^{i w} \\ e^{i w} & 0 \end{pmatrix} : \quad (18)$$

Next we consider H_{deform} . Here, we restrict ourselves to consider them on momentum transform matrix element which does not mix the two Fermi points to each other. We then expand the deformed Hamiltonian H_{deform} within the K-point and obtain

$$\begin{aligned} H_{\text{deform}} &= \sum_{a,k; i2A} V_a(r_i) f_a(k) \frac{e^{ik \cdot n_a + a}}{N_A} \mathcal{P} a_{i+a}^y \mathcal{D} i h_A^k j + h.c. \\ &= \sum_{a,k; i2A} V_a(r_i) f_a(k_F) \frac{e^{ik \cdot n_a + a}}{N_A} \mathcal{P} a_{i+a}^y \mathcal{D} i h_A^k j + h.c. \end{aligned} \quad (19)$$

The summation of the wave vector in the last equation should be recognized to be restricted in the wave vector around the K-point. Combining Eq.(18) with Eq.(19), we get an effective mass Hamiltonian,

$$\begin{pmatrix} V & 0 & e^{i w} & \Psi & A \\ e^{i w} & 0 & 0 & \Psi & A \\ e^{i w} & 0 & V_F & \mathcal{P} & e^{+i w} \\ 0 & e^{i w} & V_F & 0 & e^{i w} \end{pmatrix} : \quad (20)$$

where we have defined the Fermi velocity as $V_F = 3V a_{cc} = 2h$, $\mathcal{P} = (2h = 3a_{cc})(w_1 + iw_2)$, and $A = A_x + A_y$ where the functions $(A_x; A_y)$ are as follows:

$$\Psi A_x = V_1 \frac{1}{2} V_2 \frac{1}{2} V_3; \quad \Psi A_y = \frac{p}{2} (V_2 - V_3); \quad (21)$$

This is the explicit relationship between the modulation of the hopping integral and the deformation-induced gauge field. We call the functions $(A_x; A_y)$ or its appropriate linear combination the deformation-induced gauge field because the effects of the deformation can be included in the theory through the substitution: $p \rightarrow p + A$. This substitution is the same as that for an electromagnetic gauge field.

Here, we simplify the notation in Eq.(20) and remark on a general property of the effective Hamiltonian. We have two distinct modes, the dynamics of which are approximated by the following two effective Hamiltonians in the presence of an external electromagnetic gauge field A^{em} :

$$H_K = V_F (p + A - \frac{eA}{c}); \quad H_K^0 = V_F \begin{pmatrix} 0 & (p + A - \frac{eA}{c}) \\ (p + A - \frac{eA}{c}) & 0 \end{pmatrix}; \quad (22)$$

where we have defined $\zeta = (1; 2)$ and $^0 = (-1; 2)$, and our notation of them momentum is $p = p_1 + p_2$ ($^0 p = p_1 + p_2$) where

$$p_1 = \frac{h(2 - 1 - k_F - \zeta)}{\mathcal{C}_h j}; \quad p_2 = \frac{h(2 - 2 - k_F - T)}{\mathcal{C}_h j}; \quad (23)$$

and of the deformation-induced gauge field is $A = A_1 + A_2$ ($A = A_1 + A_2$) where

$$\begin{aligned} A_1 &= \begin{matrix} \cos & \sin & A_x \\ \sin & \cos & A_y \end{matrix} : \quad (24) \end{aligned}$$

Note that p_1 (p_2) is the momentum around (along) the axis that are measured from the K-point. As for the K'-point, k_F and ϵ_1 should change their sign and correspondingly p_1 for K'-point has an opposite sign as compared with that of K-point. Notice also the different sign for A of K and K' points, which is contrasted with the same sign for A^{em} in Eq.(22). Therefore, in the absence of the external electromagnetic gauge field, time-reversal symmetry is preserved even in the presence of deformation.

By virtue of the decomposition of Eq.(6) with the gauge coupling structure of Eq.(22), following two points become clear: (1) The ϵ_a component does not change the energy spectra of the theory because it can be eliminated by multiplying the phase of the wave function ($\epsilon_1 e^{i\frac{\pi}{n}a}$). However, it should be mentioned that a non-trivial functional form of ϵ_a gives a non-vanishing divergence of the deformation-induced gauge field: $\nabla \cdot A = \epsilon_a \neq 0$. This might correspond to the deformation potential and could cause a local (background) charge modulation [11]. An effective one-dimensional quantum field theory derived from Eq.(22) can be classified into the Tomonaga-liquid theory [12] and its framework can be used to study this effect. The analysis shows that it does not change the energy spectrum of the theory but gives only a charge density modulation. (2) The function ϵ_b works as a source of a deformation-induced magnetic field and can lead to an important physical effect. The curl part of the deformation-induced gauge field defines a deformation-induced magnetic field:

$$B_b = \epsilon_{ij} \epsilon_i A_j = r^2 \epsilon_b; \quad (25)$$

whose direction is perpendicular to a graphite surface, and a non-trivial magnetic field gives a local modulation of the energy gap which is defined in Eqs.(8) and (10).

In Eq.(7) we integrate over the circumferential coordinate (x_1) in Eq.(22). In Eq.(7), p_1^0 is determined by setting $\epsilon_1 = 0$ in Eq.(23), and ϵ_1^0 relates to the chiral index via $\epsilon_1^0 = h(2n + m) = 3i$ (x_1 indicates the closest integer to the number x : round x). Note that we have already neglected the term,

$$\epsilon_2 \int \frac{dx_1}{C_h j} \epsilon_a(x_1; x_2); \quad (26)$$

in Eq.(7) by putting a proper phase of the wave function. The coefficient of ϵ_1 works as the effective mass of a particle propagating along the axis. Then, $p_1^0 A_1^0$ is related to a position-independent mass and $m(x_2)$ expresses a local modulation of the mass. They are combined to give the local energy gap of Eq.(10).

It is valuable to note that the position-dependent mass (or local energy gap) corresponds to the existence of the

local deformation-induced magnetic field because if there remain a non-vanishing local energy gap then its first derivative about the axis direction (x_2) gives also a non-vanishing value, which corresponds to the magnetic field integrated about x_1 coordinate:

$$\epsilon_2 m(x_2) = \int \frac{dx_1}{C_h j} \epsilon_2^2 b = \int \frac{dx_1}{C_h j} B_b(x_1; x_2); \quad (27)$$

The Stokes theorem enable us to image an deformation-induced magnetic field B_k in the cylinder, which is defined by the loop integration of the deformation-induced gauge field around the axis:

$$B_k(x_2) S = \int dx_1 A_1(x_1; x_2); \quad (28)$$

where S denotes the cross sectional area of the cylinder which assumed to be constant along the axis. When the magnetic field escapes from the inside of the cylinder, it penetrates the surface of the cylinder, which corresponds to B_b on the surface (penetrating the surface) and then it change the mass of the particle (see Fig. 2).

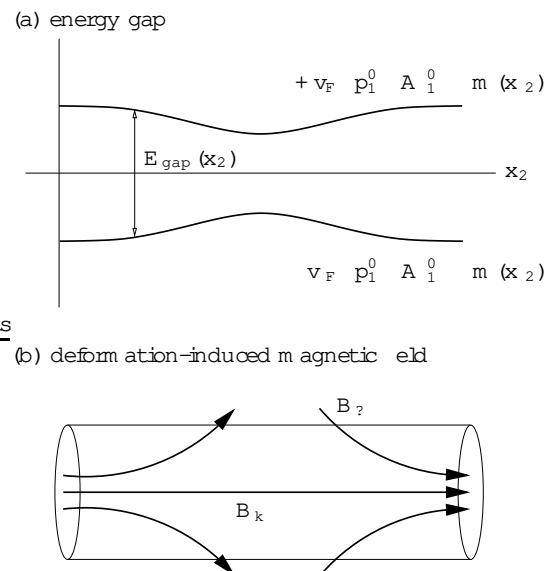


FIG. 2: Illustration of the relationship between (a) the local energy gap and (b) the corresponding deformation-induced magnetic field B_k and B_b . It is noted that this is not the usual electromagnetic magnetic field.

Let us refer to an interesting case where $p_1^0 A_1^0 m(x_2)$ changes its sign at some position. In this case, it is known that a strange solution called Jackiw-Rebbi modes [13] (electron-deformation bound states) exists at band center. Such a condition is likely to be fulfilled for the bulk part of some types of pea-pod carbon nanotubes.

IV. EXAMPLES OF DEFORMATION-INDUCED GAUGE FIELD

First we classify two types of deformation by the Slater-Koster scheme:

$$V_a(r_i) = V(a_{cc} + r_a)e(r_{i+a}) \quad e \nparallel; \quad (29)$$

which can include the fact that conducting electrons make the orbital whose wave function extends into the normal direction $e(r_i)$ of the surface. Here, $V(r)$ is a function of the bond length r ($V(a_{cc}) = V$) and $e(r_i)$ is a unit normal vector at r_i . We have assumed here that the effect of the π -bond is included into the definition of $V(r)$.

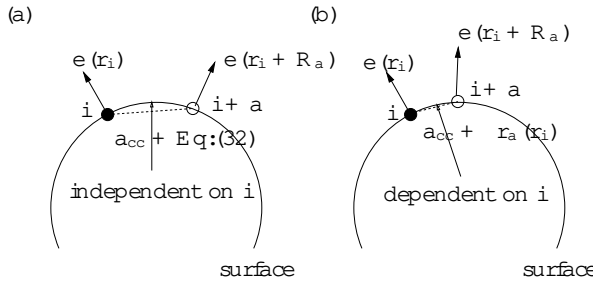


FIG. 3: A schematic diagram of a deformed surface of the two-dimensional graphite sheet. In these diagrams, only two sites (and) are depicted. We denote by $a_{cc} + r_a$ direct distance between them. We classify (a) as bond bending type, (b) as bond stretching type in this paper. In the left inset (a), the direct distance is given by $a_{cc} + \text{Eq.(32)}$, and in the right inset (b), it is not related to the normal vector.

$e(r_i + R_a)$ can be expanded in Taylor series around $e(r_i)$,

$$e(r_i + R_a) = e(r_i) + (R_a - r)e \nparallel + \frac{1}{2}(R_a - r)(R - r)e \nparallel \quad : (30)$$

Using the normalization condition of the normal vector: $e(r_i) \cdot e \nparallel = 1$, one obtains $e(r_i) \cdot (R - r)e \nparallel = 0$, so that one can write $V_a(r_i) = V_a(r_i) - V$ as

$$V_a(r_i) = r_a(r_i)(\partial V \frac{1}{2}a_{cc}) + V \frac{1}{2}e(r_i)(R_a - r)(R - r)e \nparallel + \quad : (31)$$

where \dots denotes higher order corrections. As for nanotubes, the derivative (r) is scaled by the inverse of the circumferential length ($\mathcal{C}_h \mathcal{J}$) or of the total length ($\mathcal{J} \mathcal{L}$), depending on the direction. Therefore, we can think that, as the order estimation, the relevant energy of the second term of the right hand side of Eq.(31) is proportional to an inverse square of the circumferential length: $V a_{cc}^2 = \mathcal{C}_h \mathcal{J}^2$, which gives a small (but observable [6]) correction to the energy gap. On the other hand, the bond length modulation denoted as $r_a(r_i)$ may give a dominant contribution to the energy gap [9]. Hereafter we

type	$V_a(r_i)$	target	energy scale
bending	Eq.(33)	nanotubes	$D a_{cc}^2 = \mathcal{C}_h \mathcal{J}^2$
stretching	Eq.(35)	pea-pod etc.	$(a_{cc} \partial V \frac{1}{2}a_{cc}) r_a = a_{cc}$

TABLE I: List of deformation types and expected energy scales. The bond bending type can be applied to usual single wall nanotubes and the bond stretching type is expected to be effective for pea-pod nanotubes.

shall define two types of deformation depending on the functional form of $r_a(r_i)$.

The first type of geometry includes deformed surfaces of SWNTs, the bond length modulation between adjacent carbon atoms of which is defined by (see Fig. 3(a)),

$$r_a = \frac{a_{cc}}{12} \frac{1}{2}e(r_i)(R_a - r)(R - r)e \nparallel + \quad (32)$$

By substituting this into Eq.(31), we obtain

$$V_a(r_i) = D(R_a - r)e \nparallel (R - r)e \nparallel; \quad (33)$$

where we have introduced the constant:

$$D = \frac{1}{2} \frac{1}{12}a_{cc} \partial V \frac{1}{2}a_{cc} + V; \quad (34)$$

for the sake of convenience. Incidentally, the numerical value of D can be estimated from experimental data of Ouyang et al. [6] as $\mathcal{D} \mathcal{J} = V = 8$, with $V = 2.60$ [eV]. We classify deformed surfaces whose hopping integral is approximated by Eq.(33) with an appropriate D into bond bending deformation. The hopping integral of bond bending type is calculated from the normal vectors on the surface, which means that we only need to parameterize the surface and do not need any microscopic calculation to obtain the hopping integral. Notice that we have assumed in the above that the (indirect) distance between two adjacent atoms defined by the line integral of the differential line element on a deformed graphite surface is fixed by a_{cc} and is independent on its position. This defined a type of geometry which has a curved surface.

An another type of deformation, in which dominant contribution to $V_a(r_i)$ comes from a change of the bond length. For this type, the hopping integral is well approximated by the first term of the right hand side of Eq.(31) as

$$V_a(r_i) = (\partial V \frac{1}{2}a_{cc}) r_a(r_i) + \quad : (35)$$

Equation (35) may become relevant to the conducting electrons in a pea-pod-like structure [9], where elastic strain is expected to modify the bond length. We classify deformed surfaces whose hopping integral is approximated by Eq.(35) into bond stretching deformation. The bond length (and its hopping integral) may be calculated by the first principle calculation.

Table I shows a list of deformation types. As for the bond bending type, it is expected that a typical energy of the deformed Hamiltonian is at most $D a_{cc}^2 = \mathcal{C}_h \mathcal{J}^2$, while in bond stretching type, $(a_{cc} \partial V \frac{1}{2}a_{cc}) r_a = a_{cc}$.

A . Application to Several Geometries

Here we show examples of deformation-induced gauge field and calculated results of the local energy gap. In this subsection, we calculate the deformation-induced gauge field for several geometries: nanotube and pea-pod, each of which is classified into bond bending and stretching deformation. We then apply the deformation to the local energy gap formula and compare the results with some experimental data. We also discuss briefly the effects of the external electro-magnetic gauge field and of the on-site energy.

1. narrow energy gap in metallic zigzag nanotube : bond bending type

For geometries in bond bending deformation, we may apply Eq.(33) to the deformation-induced gauge field. In this case, by substituting Eq.(17) into Eq.(33), and using Eq.(21), we obtain

$$v_F A_x = F_x^{uu} e_u - e + F_x^{uv} e_u - e + F_x^{vv} e_v - e \quad (36)$$

$$v_F A_y = F_y^{uu} e_u - e + F_y^{uv} e_u - e + F_y^{vv} e_v - e \quad (37)$$

where we have introduced the following notations:

$$\begin{aligned} F_x^{uu} &= F(p^2 + pq - \frac{1}{2}q^2); \\ F_x^{uv} &= F(2pn + qn + pm - qm); \\ F_x^{vv} &= F(n^2 + nm - \frac{1}{2}m^2); \\ F_y^{uu} &= F(p - \frac{p}{3q}(p + \frac{1}{2}q)); \\ F_y^{uv} &= F(p - \frac{p}{3}(qn + pm + qm)); \\ F_y^{vv} &= F(p - \frac{p}{3m}(n + \frac{1}{2}m)); \end{aligned} \quad (38)$$

In the above equations, we defined $F = 4^{-2}D = 3N_c^2$ and dimensionless coordinate $(u;v)$ as $C_h \cdot r = \frac{r}{\sqrt{3}} = 2\theta_u$; $T \cdot r = \frac{r}{\sqrt{3}} = 2\theta_v$, and denoted $e_u = \theta_u e$ and $e_v = \theta_v e$. The most dominant contributions to the deformation-induced gauge field are given by F_x^{uu} and F_y^{uu} terms. This is because F itself scales as inverse square of the surface area of nanotube, and $(p;q)$ scale as $\sqrt{3} \cdot (n;m)$ scale as $\sqrt{3} \cdot \sqrt{3}$. Therefore, each component scales as follows:

$$F_i^{uu} : F_i^{uv} : F_i^{vv} = \frac{a_{cc}^2}{\sqrt{3} \cdot \sqrt{3}} : \frac{a_{cc}^2}{\sqrt{3} \cdot \sqrt{3}} : \frac{a_{cc}^2}{\sqrt{3} \cdot \sqrt{3}}; \quad i = x, y; \quad (39)$$

The above scaling indicates that one may neglect the F_i^{uv} and F_i^{vv} terms as far as $\sqrt{3} \cdot \sqrt{3}$.

Since the chiral and translational indices determine each component listed in Eq.(38), specifying the normal vector on a specific surface fixes the deformation-induced gauge field completely. One can specify the surface of a tube with a constant radius by the vector: $p(u;v) = (\sqrt{3}/2 \cos u; \sqrt{3}/2 \sin u; v)$. The

unit normal vector of this surface is calculated as $e = (\cos u; \sin u; 0)$. Then we obtain $e_u \cdot e = 1; e_u \cdot e = 0; e_v \cdot e = 0$, which result in the following deformation-induced gauge field:

$$v_F A_x = F_x^{uu}; \quad v_F A_y = F_y^{uu}; \quad (40)$$

To calculate each component of Eq.(38) explicitly, let us take zigzag nanotubes (the chiral index of which is $(n;0)$) with metallic index $p_1^0 = 0$ (n is a multiple of 3) as an example. In this case Eq.(38) gives

$$F_x^{uu} = -\frac{2D}{n^2}; \quad F_y^{uu} = 0; \quad (41)$$

We apply the above to the formula of the energy gap of a metallic zigzag nanotubes and obtain $E_{\text{gap}}(v) = 2F_x^{uu} \cdot j$. Let us compare the above with an experimental result of Ouyang et al. [6]. The experiment shows an energy gap for metallic zigzag SWNTs with $n = 9; 12; 15$ can be fitted by

$$E_{\text{gap}}^{\text{exp}} = \frac{2V}{4n^2} \quad (V = 2.60 \text{ eV}); \quad (42)$$

which corresponds to the parameter $D \cdot j = V = 8$. Using the explicit form of the parameter D , we can read off the first derivative of $V(r)$:

$$a_{cc} @ V \cdot j_{cc} = \begin{cases} 9V & \text{if } D < 0 \\ 15V & \text{if } D > 0; \end{cases} \quad (43)$$

which can be used to analyze the other chiral structures and also for geometries of the bond stretching deformation.

2. pea-pod : bond stretching type

We consider a pea-pod geometry as an example of bond stretching deformation whose hopping integral strongly depends on the bond length modulation. As for some (encapsulated metallic fullerenes) pea-pod-like structure [9], elastic strain is expected to modify the bond length. We do not attempt to calculate the bond length for such systems using first principle calculation but instead would like to estimate the bond length modulation which is necessary to explain an observed local energy gap modulation within our theoretical framework.

We consider zigzag nanotubes $(n;0)$ with constant radius and assume that $A_1 = A_x$ depends only on the axis coordinate. In this case, we can simplify the formula of the energy gap as

$$E_{\text{gap}}(y) = 2v_F \cdot p_x^0 \cdot A_x(y); \quad (44)$$

From Eqs.(21) and (35), the deformation-induced gauge field around the axis can be written as

$$\Psi A_x(y) = (\theta V \cdot j_{cc}) \cdot r_1(y) - \frac{1}{2} r_2(y) - \frac{1}{2} r_3(y); \quad (45)$$

It is reasonable to suppose that the bonds, pointing three different directions, are related to each other because the modulation generates a force between the adjacent atoms. For zigzag, we assume the following relation: $r_2(y) = r_3(y) = \frac{1}{2} r_1(y)$, which gives an equilibrium con guration and preserves the rotational symmetry around the axis. In this case, the energy gap formula becomes

$$E_{\text{gap}}(y) = 2 v_F p_x^0 - \frac{1}{2} (a_{\text{cc}} @ V j_{\text{cc}}) \frac{r_1(y)}{a_{\text{cc}}} ; \quad (46)$$

where the first term on the right hand side can be given for zigzag nanotubes with chiral index $(n;0)$ as

$$v_F p_x^0 = V \frac{2 \frac{p}{3}}{n} \frac{2n}{3} \frac{2n}{3} : \quad (47)$$

In order to achieve an observed energy gap modulation of the order of 0.4 eV [9], the maximum of the bond-length modulation should be of the order of $r_1^{\text{max}}/a_{\text{cc}}=50$, where we have used the upper case of Eq.(43). Although this quantity was fixed by the experimental date of Ouyang et al [6], it can be estimated by another scheme [14] as $(a_{\text{cc}} @ V j_{\text{cc}}) = 3V$. In this case, the maximum bond length modulation should be about $a_{\text{cc}}=20$. In any case, the small bond length modulation gives a rather strong contribution to the local energy gap.

3. co-existence of deformation-induced and electro-magnetic gauge field

It is valuable to note that the deformation-induced gauge field can give a much larger energy scale as compared to the usual (magnetic) gauge field. To show that, we consider the relationship between the deformation-induced gauge field and an external magnetic field applied to the perpendicular to the axis. Such an external magnetic field can be derived from an external gauge field:

$$A_1^{\text{em}} = 0; A_2^{\text{em}} = \frac{eB^{\text{em}} \mathcal{J}_h j}{2} \sin u: \quad (48)$$

For practical range of an external magnetic field (10 Tesla), the deformation-induced gauge field can give a much larger energy scale than that of the external gauge field:

$$v_F \frac{eB^{\text{em}} \mathcal{J}_h j}{2} \approx 10^9 \frac{\mathcal{J}_h j}{a_{\text{cc}}} [B^{\text{em}} = \text{Gauss}]: \quad (49)$$

Therefore, for a typical SWNTs of $\mathcal{J}_h j = 10a_{\text{cc}}$, the effects of the external magnetic field on the energy gap can be safely ignored even for a magnetic field of the order of 10 Tesla. Note also that, when we consider the one-dimensional model, it is shown that the external field does not change the energy gap because $\partial_u A_1^{\text{em}} = 0$ and $\partial_u A_2^{\text{em}} = 0$, which is contrasted to the deformation-induced gauge field.

4. on-site energy : asymmetry between two sublattice

Let us briefly comment on the on-site interaction. The on-site energy is defined by

$$H_{\text{site}} = \sum_i (r_i) a_i^y a_i; \quad (50)$$

where (r_i) denotes the on-site energy. The constant component of the on-site energy determines the origin of the energy and inactive for the dynamics. On the other hand, its modulation part can give physical effects on the conducting electrons. The modulation can be divided into two parts: symmetric for two sublattice part and asymmetric one. They appear in the low energy Hamiltonian as the component of $\mathbb{1}$ (identity matrix) and of σ_3 respectively [15]:

$$H_K = v_F (p - A) + G(r) \mathbb{1} + P(r) \sigma_3: \quad (51)$$

The former $G(r)$ works as the local electrical potential and the latter $P(r)$ gives asymmetric potential between two sublattice. $G(r)$ does not change the energy gap of the theory, however, $P(r)$ does. The local energy gap along the axis can be calculated by the dimensional reduction as follows:

$$E_{\text{gap}}(x_2) = 2 v_F^2 p_1^0 - \frac{dx_1}{\mathcal{J}_h j} A_1 + \frac{dx_1}{\mathcal{J}_h j} P: \quad (52)$$

V. MIXING OF FERMIPONTS

Up to now we have disregarded the matrix element that causes a mixing of two Fermi points K and K' , each of which is of the order of $V_a (2k_F)$ (We set the Fermi velocity unity: $v_F = 1$, in this section). Let us begin by introducing the Schrodinger equation, the Hamiltonian of which is given by

$$i\hbar \frac{\partial}{\partial t} \begin{pmatrix} K \\ K^0 \end{pmatrix} = \begin{pmatrix} H_K & 0 \\ 0 & (H_{K^0})^0 \end{pmatrix} \begin{pmatrix} K \\ K^0 \end{pmatrix}; \quad (53)$$

where we have defined $(H_{K^0})^0$ as H_{K^0} (Eq.22) with the following replacement: $(p_1; p_2) \rightarrow (-p_1; p_2)$. Thus, each diagonal block is respectively given by

$$H_K = \begin{pmatrix} 1 (p_1 & A_1 & A_1^{\text{em}}) & 2 (p_2 & A_2 & A_2^{\text{em}}) \\ 2 (p_1 & A_1 + A_1^{\text{em}}) & 1 (p_2 & A_2 + A_2^{\text{em}}) \end{pmatrix};$$

$$(H_{K^0})^0 = \begin{pmatrix} 1 (p_1 & A_1 & A_1^{\text{em}}) & 2 (p_2 & A_2 & A_2^{\text{em}}) \\ 2 (p_1 & A_1 + A_1^{\text{em}}) & 1 (p_2 & A_2 + A_2^{\text{em}}) \end{pmatrix};$$

Roughly speaking, p_1 measures the difference between the momenta (around the axis) for K and K' states. The $\mathbb{1}$ terms work as the mass term (or energy gap) when we consider an effective one-dimensional model. In this respect, we note the different signs for an external magnetic field A_1^{em} . Since A_1^{em} can be tuned by a magnetic field along the axis, it can make an asymmetry of

the mass of two modes [16], in other words, can break T-symmetry.

The matrix defined above is acting on the four component wave function:

$$\begin{matrix} 0 & K & 1 \\ & \begin{matrix} K \\ A \\ K \\ B \\ B \\ C \\ K \\ A \\ A \\ K \\ B \\ K \\ B \end{matrix} \\ K & \begin{matrix} B \\ B \\ C \\ K \\ A \\ A \\ K \\ B \\ K \\ B \end{matrix} \\ 0 & \begin{matrix} (H_K)_{12} & 0 & 2b_1 & 1 \\ 0 & 2b_2 & 0 & C \\ 0 & 2b_2 & 0 & (H_K^0)_{12}^0 \\ 2b_1 & 0 & (H_K^0)_{21}^0 & 0 \end{matrix} \end{matrix} ; \quad (54)$$

where two component of K (K^0) corresponds to the wave functions at the two sublattices, A and B. The A component couples to the wave functions on the B-sublattice: B and B , and the coupling between A and B expresses the mixing effect. Therefore, a general dynamics (except for the topological defects mentioned below) can be described by the following Hamiltonian:

$$\begin{matrix} 0 & 0 & (H_K)_{12} & 0 & 2b_1 & 1 \\ & B & (H_K)_{21} & 0 & 2b_2 & 0 & C \\ & 0 & 0 & 2b_2 & 0 & (H_K^0)_{12}^0 & A \\ 2b_1 & 0 & 0 & (H_K^0)_{21}^0 & 0 & 0 \end{matrix} ; \quad (55)$$

where $b = (b_1, b_2)$ are some complex functions.

The mixing of Fermi points may cause a strong effect on the dynamics especially in the presence of pentagon or heptagon in the surface [17]. We try to construct a low energy effective model including the effects of a topological defect, and also of the surface deformation. For that purpose, we first note that the effective dynamics of Eq.(55) can be expressed as a special case of the following Schrodinger equation:

$$D = 0; \text{ where } D = (p - A^0)_0 - A^i_i; \quad (56)$$

where the summation variable should be understood to take $2, 0, 1, 2, g$, and D are the covariant momentum. A^i is a generalization of the previously defined deformation-induced gauge field and i is the Pauli matrices (0 is the identity element) acting on the wave functions $(K, K^0)^t$. It is noted that we have defined $=$, and $p_0 = i\hbar\partial_t$ (t is time variable). The Schrodinger equation is formally equivalent to the Weyl equation in U(1) Abelian and SU(2) non-Abelian deformation-induced gauge field.

The Hamiltonian of Eq.(55) can be obtained by setting the generalized gauge field in Eq.(56) as,

$$\begin{aligned} A_1^3 &= A_1^{\text{ex}}; A_2^0 = A_2^{\text{ex}}; \\ A_1^0 &= A_1; A_2^3 = A_2; \\ A_1^1 &= \langle (b_1 + b_2); A_1^2 = (b_1 + b_2); \\ A_2^2 &= \langle (b_1 - b_2); A_2^1 = (b_1 - b_2); \end{aligned} \quad (57)$$

and other components zero. Let us comment on the relationship between pentagon or heptagon and the non-Abelian deformation-induced gauge field. The main contribution from a pentagon or a heptagon is the interchange of the wave functions of two Fermi points. It happens when a low energy electron turns around the

topological defect [17], which can be expressed by a non-vanishing time component of the matrix element of 1 or 2 part:

$$\begin{matrix} 0 & 0 (A_0^1 & iA_0^2) & K \\ 0 (A_0^1 + iA_0^2) & 0 & K^0 \end{matrix} : \quad (58)$$

This is because a pentagon (heptagon) makes a coupling between A and A^0 or between B and B^0 . Hence, the local dynamics of the low energy conducting electron on a deformed (graphite) surface is governed by Eq.(56) and the lattice structure fixes the Abelian and non-Abelian deformation-induced gauge field. Notice that not all the information of the deformation-induced gauge field can lead to a physical effect, as was shown in the non-mixing case. The magnetic field of the non-Abelian deformation-induced gauge field is given by the field strength of the gauge field:

$$F_{12}^k = \partial_1 A_2^k - \partial_2 A_1^k + \epsilon_{ijk} A_1^i A_2^j; \quad (59)$$

When the mixing effect is neglected, the magnetic field of the U(1) gauge field component $F_{12}^0 = \partial_1 A_2^0 - \partial_2 A_1^0$ reproduces the local energy gap obtained in section II. Since the local physical quantity should be related to a gauge invariant quantity (for example, $\epsilon_k (F_{12}^k)^2$), one may expect that a rich electric and magnetic properties in the deformed systems can be clarified in terms of the generalized deformation-induced gauge field.

V I. DISCUSSIONS

The main result of the local energy gap (Eq.10) is determined only by the conformation of the deformation-induced gauge field. This is due to the special energy dispersion relation of the graphene sheet, which enables us to predict several important physical consequences without solving the Hamiltonian explicitly but with the gauge field conformation itself. To understand the conformation of the deformation-induced gauge field, we have classified the geometries into two categories: bond bending and stretching deformation. For bending type, one can extract the gauge field from the geometrical information given by the normal vector as we have done in section IV A 1, where no microscopic theory is necessary to calculate the field conformation. On the other hand, for stretching type, one needs a microscopic theory that is able to predict the bond-length or the gauge field in order to calculate the local energy gap (section IV A 2). We can make a qualitative analysis of bond stretching type using a microscopic model and compare it with our local energy gap formula, which will be reported elsewhere.

When we consider the mixing effect due to short range interaction, we should generalize the geometry-induced gauge field from Abelian to non-Abelian field. Constructing a general low energy theory is of prime importance because a general deformation may generate a topological defect such as a pentagon or heptagon, which can

mix the wave functions at two Fermi points. In addition, one can consider a higher genus material, the kinematics of which is obscure [18]. A possible way to examine such a material is to extract a useful information from a dynamical model.

Finally, we comment on the wave functions in the nanotubes with local energy gap modulation. Notice that we did not solve the effective Hamiltonian Eq.(22), but extracted the energy gap along the axis by considering the spectrum of the effective one-dimensional theory (Eq.7), which is obtained by the dimensional reduction. Solving the equation for a general A without the dimensional reduction would be difficult even in the absence of the mixing because the eigenfunctions of the Hamiltonian: $H_K = E$ should also satisfy [19]:

$$H_K^2 = (p - A)^2_0 + hB_3^i = E^2 ; \quad (60)$$

where we have set $v_F = 1$ and $A^{\text{em}} = 0$. The spectrum of the first term on the right hand side is known to be quite non-trivial even for a case of simple vortex configurations [20]. Furthermore, it is already hard to solve the one-dimensional Hamiltonian because of the local modulation mass term. The nature of the wave function would be important for investigating the possibility of the "energy gap engineering" which needs a multiple quantum dots prepared by the local modulation of the energy gap.

V II. CONCLUSION

In the present paper, we have examined the effects of surface deformation on the ground-state of the conducting electrons using the nearest-neighbor tight-binding Hamiltonian. In the framework of the effective mass theory, we have clarified the relationship between the local deformation of the lattice and the local energy gap along the axis in terms of the deformation-induced magnetic field. We have constructed the effective theory describing the dynamics on a generalized surface including the topological defects that can cause the mixing of the two Fermi points. The theory is formally equivalent to the Weyl equation in U(1) Abelian and SU(2) non-Abelian deformation-induced gauge field.

Acknowledgments

K. S. is supported by a fellowship of 21st century COE program of international center of research and education for materials of Tohoku University. R. S. acknowledges a Grant-in-Aid (No. 13440091) from the Ministry of Education, Japan.

[1] S. Iijima, *Nature* 354, 56 (1991).
 [2] R. Saito, G. D. Dresselhaus, and M. S. Dresselhaus, *Physical Properties of Carbon Nanotubes*, Imperial College Press, London (1998).
 [3] J.W. G. W. Wildeoer, L.C. Venema, A.G.R. Zandbergen, R.E. Smalley, and C.D. Dekker, *Nature* 391, 59 (1998); T.W. Odom, J. Huang, P. Kim, and C.M. Lieber, *Nature* 391, 62 (1998).
 [4] J.C. Slonczewski and P.R. Weiss, *Phys. Rev.* 109, 272 (1958).
 [5] C.L. Kane and E.J. Mele, *Phys. Rev. Lett.* 78, 1932 (1997).
 [6] M. Ouyang, J. Huang, C.L. Cheung, and C.M. Lieber, *Science* 292, 27 (2001).
 [7] A. Kleiner and S. Eggert, *Phys. Rev. B* 64, 113402 (2001); 63, 73408 (2001); L.F. Chibotaru, S.A. Bovin, and A. Ceulemans, *Phys. Rev. B* 66, 161401 (2002).
 [8] T. Ando, T. Nakanishi, and R. Saito, *J. Phys. Soc. Jpn.* 67, 2857 (1998).
 [9] J. Lee, H. Kim, S.-J. Kahng, G. Kim, Y.-W. Son, J. Ihm, H. Kato, Z.W. Wang, T. Okazaki, H. Shinohara, and Y. Kuk, *Nature* 415, 1005 (2002).
 [10] J.M. Luttinger and W. Kohn, *Phys. Rev.* 97, 869 (1955).
 [11] H. Suzuura and T. Ando, *Phys. Rev. B* 65, 235412 (2002).
 [12] S. Tomonaga, *Prog. Theo. Phys.* 5, 544 (1950).
 [13] R. Jackiw and C. Rebbi, *Phys. Rev. D* 13, 3398 (1976).
 [14] C.H. Xu, C.Z. Wang, C.T. Chan, and K.M. Ho, *J. Phys.: Condens. Matter* 4, 6047 (1992); L.G. Godwin, A.J. Skinner, and D.G. Pettifor, *Europhys. Lett.* 9, 701 (1989).
 [15] N.A. Viet, H.A. Jiki, and T. Ando, *J. Phys. Soc. Jpn.* 63, 3036 (1994).
 [16] H.A. Jiki and T. Ando, *J. Phys. Soc. Jpn.* 62, 2470 (1993), *Solid State Comm.* 102, 135 (1997); S. Zaric, G.N. Ostojic, J. Kono, X. Wei, M.S. Strano, V.C. Moore, R.H. Hauge, and R.E. Smalley, *arXiv:cond-mat/0308233*.
 [17] J. Gonzalez, F. Guinea, and M.A. Vozmediano, *Phys. Rev. Lett.* 69, 172 (1992), *Nucl. Phys. B* 406, 771 (1993); H.M. Atsumiura and T. Ando, *J. Phys. Soc. Jpn.* 67, 3542 (1998), 70, 2657 (2001); P.E. Lammer and V.H. Crespi, *Phys. Rev. Lett.* 85, 5190 (2000).
 [18] K. Sasaki, Y. Kawazoe, and R. Saito, *arXiv:cond-mat/0310292*, to be published in *Phys. Lett. A*.
 [19] R. Jackiw, *Phys. Rev. D* 29, 2375 (1984).
 [20] Y. Aharonov and D. Bohm, *Phys. Rev.* 115, 485 (1959); R. Jackiw, *Ann. Phys.* 201, 83 (1990); Y. Nambu, *Nucl. Phys. B* 579, 590 (2000).